INTERNATIONAL JOURNAL FOR NUMERICAL METHODS IN FLUIDS
Int. J. Numer. Meth. Fluids 2008; **56**:1457–1463
Published online 6 November 2007 in Wiley InterScience (www.interscience.wiley.com). DOI: 10.1002/fld.1647

Conservative and non-conservative arbitrary Lagrangian–Eulerian forms for ventricular flows

D. A. Nordsletten[1, 2, *, †], P. J. Hunter[2] and N. P. Smith[1, 2]

[1]*Oxford Computing Laboratory, University of Oxford, Parks RD, Oxford OX1 3JP, U.K.*
[2]*Bioengineering Institute, University of Auckland, Uniservices Building, Level 6, 70 Symonds Street, New Zealand*

SUMMARY

Blood flow through the heart is driven by a complex motion of the endocardial heart wall, where dilation or contraction results in filling and ejection. Boundary-driven flows of this type are inherently sensitive to conservation principles. Considering the finite element approach to the arbitrary Lagrangian–Eulerian (ALE) form of the Navier–Stokes equations, we present analysis addressing critical assumptions concerning conservation and numerical approximation which affect the accuracy and stability of ALE schemes for boundary-driven flows. Copyright © 2007 John Wiley & Sons, Ltd.

Received 2 April 2007; Revised 26 July 2007; Accepted 28 September 2007

KEY WORDS: Navier–Stokes; finite element; numerical analysis; blood flow

1. INTRODUCTION

The use of computational fluid mechanics is emerging as a key component to furthering our understanding of cardiac function both theoretically and clinically. A number of mathematical models, using immersed boundary [1, 2], finite difference [3], finite volume [4, 5], and finite element (FE) techniques [6], have been presented in the literature on this application. Of these models which consider flow, the arbitrary Lagrangian–Eulerian (ALE) form of the Navier–Stokes equation (NSE) is the predominant formulation.

The moving description on which ALE conservation laws are posed is particularly attractive for boundary-driven flow problems. However, embedded within this form are a number of important intricacies. Prior to solving complex boundary-driven flow problems, such as those within the heart chambers, it is pertinent to carefully consider the numerical implementation of these forms.

*Correspondence to: D. A. Nordsletten, Oxford Computing Laboratory, University of Oxford, Parks RD, Oxford OX1 3JP, U.K.
†E-mail: david.nordsletten@dpag.ox.ac.uk

Contract/grant sponsor: Whitaker Fellowship, University of Auckland Doctoral Scholarship, Wellcome Trust

In the remainder of this paper, we develop the conservative/non-conservative ALE form for a Newtonian fluid in both strong and weak forms, analyzing their spatial and temporal complexities. The ramification of these results, in terms of stability and accuracy, is finally highlighted with numerical results for both a test problem and cardiac ventricular simulations.

2. CONSERVATIVE AND NON-CONSERVATIVE ALE–NSE FORMS

Consider the general physical domain, $\Omega_t \subset \mathbb{R}^d \times [0,T]$ (with boundary Γ_t), over which we consider the fluid problem, and an arbitrary computational domain $\Lambda \subset \mathbb{R}^d$. We will refer to x and η as the spatial coordinates of Ω_t and Λ, respectively. These domains are related by a bijective mapping, $\mathscr{P}_t : \Lambda \to \Omega_t$, which maintains boundary congruity through time (i.e. $\mathscr{P}_s \circ \mathscr{P}_t^{-1}(\Gamma_t) := \Gamma_s \ \forall (s,t) \in [0,T]$). Further, the mapping has a deformation gradient tensor $\mathscr{F}_t := \nabla_\eta \mathscr{P}_t$ and mapping Jacobian $\jmath_t := \det|\mathscr{F}_t|$ (i.e. $\mathrm{d}x = \jmath_t \, \mathrm{d}\eta$). Let $\mathbf{v}, \mathbf{w} : \Lambda \times [0,T] \to \mathbb{R}^d$ and $p : \Lambda \times [0,T] \to \mathbb{R}$ be the fluid velocity, domain velocity ($\mathbf{w} := \partial_t \mathscr{P}_t$), and pressure, respectively (where $\partial_t(\cdot) = (\partial/\partial t)(\cdot)|_{x=\mathscr{P}_t(\eta)}$). The NSE, which assumes a Newtonian stress law [7], $\sigma = -p\mathbf{I} - \lambda \nabla_x \cdot \mathbf{v} + \mu(\nabla_x \mathbf{v} + \mathbf{v}\nabla_x)$, and constant density ρ with respect to space and time, is given by the following equations[‡]

$$\rho \partial_t \mathbf{v} + \rho(\mathbf{v} - \mathbf{w}) \cdot \nabla_x \mathbf{v} + \nabla_x p - \mu \Delta_x \mathbf{v} = \rho \mathbf{v}\left(\nabla_x \cdot (\mathbf{w} - \mathbf{v}) - \jmath_t^{-1} \partial_t \jmath_t\right) + (\lambda + \mu) \nabla_x \nabla_x \cdot \mathbf{v} \tag{1}$$

$$\nabla_x \cdot \mathbf{v} = -\jmath_t^{-1} \partial_t \jmath_t + \nabla_x \cdot \mathbf{w} \tag{2}$$

where λ is the bulk viscosity (commonly taken as $\lambda = -2\mu/3$) and μ the viscosity. Unlike the Eulerian form of NSE, the general ALE form does not result in the identity $\nabla_x \cdot \mathbf{v} = 0$ unless the RHS of Equation (2) i.e. the space conservation law (SCL) is equivalently zero [8]. A consequence of the ALE form, the terms on the RHS of Equations (1) and (2) account for sources or sinks in space due to domain movement. When these terms are removed on the LHS [8], Equations (1) and (2) are equivalent to the so-called non-conservative forms [6].

The conservative weak form (Equations (3) and (4)) is derived by the integration of Equations (1) and (2) over Λ and the time interval $I = [m,n]$, while the non-conservative weak form (Equations (5) and (6)) is integrated over the Λ at a time point n. Typically, the RHS of Equation (6) is neglected as zero, which is generally applicable under exact integration.

$$\begin{aligned} &\rho(\mathbf{v},\mathbf{u})_{\Omega_n} - \rho(\mathbf{v},\mathbf{u})_{\Omega_m} + \rho(\mathbf{v}\cdot\nabla_x\mathbf{v},\mathbf{u})_{\Omega_I} - \rho(\mathbf{w}\cdot\nabla_x\mathbf{v},\mathbf{u})_{\Omega_I} - (p,\nabla_x\cdot\mathbf{u})_{\Omega_I} + \mu(\nabla_x\mathbf{v},\nabla_x\mathbf{u})_{\Omega_I} \\ &\quad + \mathscr{B}_{\Gamma_I}(\mathbf{v},p,\mathbf{u}) = \rho(\mathbf{v}\nabla_x\cdot\mathbf{w},\mathbf{u})_{\Omega_I} - \rho(\mathbf{v}\nabla_x\cdot\mathbf{v},\mathbf{u})_{\Omega_I} - ((\lambda+\mu)\nabla_x\cdot\mathbf{v},\nabla_x\cdot\mathbf{u})_{\Omega_I} \end{aligned} \tag{3}$$

$$(\nabla_x \cdot \mathbf{v}, z)_{\Omega_I} = (z,1)_{\Omega_m} - (z,1)_{\Omega_n} + (\nabla_x \cdot \mathbf{w}, z)_{\Omega_I} \tag{4}$$

$$\begin{aligned} &\rho(\partial_t\mathbf{v},\mathbf{u})_{\Omega_n} + \rho(\mathbf{v}\cdot\nabla_x\mathbf{v},\mathbf{u})_{\Omega_n} - \rho(\mathbf{w}\cdot\nabla_x\mathbf{v},\mathbf{u})_{\Omega_n} - (p,\nabla_x\cdot\mathbf{u})_{\Omega_n} + \mu(\nabla_x\mathbf{v},\nabla_x\mathbf{u})_{\Omega_n} \\ &\quad + \mathscr{B}_{\Gamma_n}(\mathbf{v},p,\mathbf{u}) = -\rho(\mathbf{v}\nabla_x\cdot\mathbf{v},\mathbf{u})_{\Omega_n} - ((\lambda+\mu)\nabla_x\cdot\mathbf{v},\nabla_x\cdot\mathbf{u})_{\Omega_n} \end{aligned} \tag{5}$$

$$(\nabla_x \cdot \mathbf{v}, z)_{\Omega_n} = -\partial_t(z,1)_{\Omega_n} + (\nabla_x \cdot \mathbf{w}, z)_{\Omega_n} \tag{6}$$

[‡]For completeness, we assume temperature independence and constant viscosity coefficients.

DOI: 10.1002/fld

Where $(\cdot,\cdot)_{V_s}$, given generally in Equation (7),[§] relates to the L^2-inner product and $\mathscr{B}_{V_I}(\mathbf{v}, p, \mathbf{u}) = ((p\mathbf{I} - \mu\nabla_x\mathbf{v} - (\lambda+\mu)\nabla_x\cdot\mathbf{v}\mathbf{I})\cdot\mathbf{n}, \mathbf{u})_{V_I}$ ($\mathbf{n}$ being the time-varying boundary normal of Γ_I).

$$(\mathbf{a},\mathbf{b})_{V_s} = \int_{V_s} \mathbf{a}\star\mathbf{b}\,\mathrm{d}x, \quad (\mathbf{a},\mathbf{b})_{V_I} = \int_I (\mathbf{a},\mathbf{b})_{V_\xi}\,\mathrm{d}\xi \tag{7}$$

Here $\mathbf{v},\mathbf{u}\in\mathbf{H}^1(\Lambda)$, $\mathbf{w}\in\mathbf{L}^2(\Lambda)$, and $p, z\in L^2(\Lambda)$ at any discrete time points $m, n\in[0,T]$ subject to conditions in Equations (3) and (4). Thus, the state variables $\mathbf{v}, \mathbf{w}$, and p must be mapped ($x = \mathscr{P}_I(\eta)$) to apply the integral and gradient operators in Ω_I. This rather straightforward result has significant implications for the evaluation of the associated terms over space and time.

2.1. Spatio-temporal complexity of the Galerkin weak form

Dealing with approximate FE solutions to our state variables, we use polynomial bases (subspaces of $\mathbf{H}^1(\Lambda)$, $\mathbf{L}^2(\Lambda)$, or $L^2(\Lambda)$) to describe the spatial and/or temporal variation. Although typically thought of in some discrete sense, we may consider an order of temporal complexity (the discrete case being zero order in time). We assume that $\mathscr{P}_t\sim\mathscr{O}(\kappa_\mathscr{P};\tau_\mathscr{P})$, $\widehat{\mathbf{v}}\sim\mathscr{O}(\kappa_\mathbf{v};\tau_\mathbf{v})$, $\widehat{\mathbf{w}}\sim\mathscr{O}(\kappa_\mathscr{P};\tau_\mathscr{P}-1)$, and $\widehat{p}\sim\mathscr{O}(\kappa_p;\tau_p)$ are of the given orders in space and time, respectively. The bases for $\mathbf{u}$ and z being constant with respect to ∂_t (i.e. a fixed point in Λ), are thus $\mathbf{u}\sim\mathscr{O}(\kappa_\mathbf{v};0)$ and $z\sim\mathscr{O}(\kappa_p;0)$. Further, $\mathscr{F}_t\sim\mathscr{O}(s_\mathscr{P};\tau_\mathscr{P})$ and $\mathscr{J}_t\sim\mathscr{O}(ds_\mathscr{P};d\tau_\mathscr{P})$, where $s_\mathscr{P}=\kappa_\mathscr{P}$ unless the basis is reduced to a full order under differentiation (in this case $s_\mathscr{P}=\kappa_\mathscr{P}-1$).[¶]

As Ω_t varies in time, both the integral and gradient operators assume a time-dependent relation with their static Λ equivalents (Equation (8)). Thus, spatial integration adds a spatio-temporal complexity of $\mathscr{O}(ds_\mathscr{P};d\tau_\mathscr{P})$ to the integrand. Owing to its relation to the deformation gradient tensor (Equation (8)), all spatial gradients with respect to ∇_x inherit additional spatial and temporal complexity of $\mathscr{O}((d-1)s_\mathscr{P})/\mathscr{O}(ds_\mathscr{P})$ and $\mathscr{O}((d-1)\tau_\mathscr{P})/\mathscr{O}(d\tau_\mathscr{P})$, respectively.

$$\int_{\Omega_t}\mathrm{d}\mathbf{x} := \int_\Lambda \mathscr{J}_t\,\mathrm{d}\eta, \quad \mathscr{F}_t^{-\mathrm{T}}\nabla_\eta := \nabla_x \tag{8}$$

Using these results, we may determine the spatial and temporal integral complexities of all terms based on the complexity of the mapping and state variables selected (Table I). It is clear that with complex element types, mapping functions and high-order spatio-temporal interpolations, the cost of calculating NSE terms increases significantly. Additionally, the viscous stress terms that include second-order differential operators in strong form give rise to irreducible rational functions. In many cases, the use of tetrahedral elements reduces the viscous term denominator to an element-wise constant spatial function. A similar reduction, for the conservative form, cannot be conducted for temporal accuracy, as this would imply the ALE mapping, $\mathscr{P}_t$, to be constant (i.e. describe an Eulerian frame). From Equation (4), we deduce that given $\widehat{\mathbf{w}}$, $\tau_\mathbf{v} > \tau_\mathscr{P} - 1$ is required for exactness. The weak form of mass conservation in Equations (4) and (6) also illustrates that the RHS is only zero when the terms are integrated precisely in time [9]. Thus to conserve mass, we must use appropriate integration schemes. This result is important and precedes any reductions that suppose a divergence-free velocity field. The ramifications for violating this result can be significant both in terms of solution accuracy and stability.

[§] The $\star$ operator of Equation (7) assumes multiplication, $\cdot$, : for scalar, vector, and tensors $\mathbf{a}$ and $\mathbf{b}$, respectively.
[¶] Typically, $s_\mathscr{P}=\kappa_\mathscr{P}-1$ for d-simplex elements and $s_\mathscr{P}=\kappa_\mathscr{P}$ for quadrilateral and hexahedral elements.

DOI: 10.1002/fld

Table I. ALE–NSE weak form spatio-temporal complexity of the conservative (c) and non-conservative (nc) forms.

Term (c/nc)	Spatial order (c,nc)	Temporal order (c)
$(3)-1,2(5)-1,6$	$\mathcal{O}(2\kappa_{\mathbf{v}}+ds_{\mathscr{P}})$	—
$(3)-3,8(5)-2$	$\mathcal{O}(2\kappa_{\mathbf{v}}+s_{\mathbf{v}}+(d-1)s_{\mathscr{P}}))$	$\mathcal{O}(2\tau_{\mathbf{v}}+(d-1)\tau_{\mathscr{P}})$
$(3)-4,7(5)-3$	$\mathcal{O}(\kappa_{\mathbf{v}}+s_{\mathbf{v}}+(d-1)s_{\mathscr{P}}+\kappa_{\mathscr{P}})$	$\mathcal{O}(\tau_{\mathbf{v}}+d\tau_{\mathscr{P}}-1)$
$(3)-5(5)-4$	$\mathcal{O}(\kappa_p+s_{\mathbf{v}}+(d-1)s_{\mathscr{P}})$	$\mathcal{O}(\tau_p+(d-1)\tau_{\mathscr{P}})$
$(3)-6,9(5)-5,7$	$\frac{\mathcal{O}(2s_{\mathbf{v}}+2(d-1)s_{\mathscr{P}})}{\mathcal{O}(ds_{\mathscr{P}})}$	$\frac{\mathcal{O}(\tau_{\mathbf{v}}+2(d-1)\tau_{\mathscr{P}})}{\mathcal{O}(2\tau_{\mathscr{P}})}$
$(4)-1(6)-1$	$\mathcal{O}(\kappa_p+s_{\mathbf{v}}+(d-1)s_{\mathscr{P}})$	$\mathcal{O}(\tau_{\mathbf{v}}+(d-1)\tau_{\mathscr{P}})$
$(4)-2,3(6)-2$	$\mathcal{O}(\kappa_p+ds_{\mathscr{P}})$	—
$(4)-4(6)-3$	$\mathcal{O}(\kappa_p+ds_{\mathscr{P}})$	$d\tau_{\mathscr{P}}-1$

Note: Numbers correspond to terms as they appear in the indicated equations, excluding the boundary integrals. We note that the spatio-temporal complexity of $\mathscr{B}_{V_l}(\mathbf{v}, p, \mathbf{u})$ has equivalent order, term-wise, to those from which it arose through integration by parts.

2.2. *Galerkin ALE–NSE FE method*

The method developed solves the fully coupled ALE–NSE conservative and non-conservative forms over linear/curvilinear d-simplex/polytopes, $\mathscr{T}_\Lambda/\mathscr{H}_\Lambda$, of Ω_t under the mapping $\mathscr{P}_t$. An implicit first-order backward Euler approach was taken due to more favorable stability [10]. The velocity and pressure test spaces used are the general Taylor–Hood basis, which satisfy the inf–sup condition [11].

Using Table I, spatial and temporal quadratures were selected to integrate (to machine precision) all terms in conservative and non-conservative forms, excluding the viscous stress term. As we employed a backward Euler scheme, a 2-point Gaussian quadrature was sufficient for all but the viscous terms in the conservative form (Q_t^2). A 5-point quadrature (Q_t^5) provided the best results, as higher quadratures incurred more significant computational cost with little or no improvement in calculation accuracy. We posed the fully coupled problem by analytically calculating the Jacobian matrix and solving the non-linear system with a global Newton–Raphson iteration [12]. MUMPS[‖] and BommerAMG[**] were selected to solve the linearized matrix system.

3. RESULTS AND DISCUSSION

The significance of those terms that delineate the non-conservative (nc) and fully conservative (c) forms, the SCL as well as the impact of their calculation, is unquantified in the literature. To illustrate their importance, we consider the problem of constant axial flow through a rectangular hexahedron under transient deformation. Various inhomogeneous deformations were applied (such that $\nabla_x \cdot \widehat{\mathbf{w}} \neq 0$) by adding sinusoidal contractions and expansions of the domain in each dimension. Dirichlet ($\widehat{\mathbf{v}} = U(1,0,0)^{\mathrm{T}}$ at the inlet and side walls), symmetry (top and bottom), and zero normal

[‖] Available from http://graal.ens-lyon.fr/MUMPS/avail.html.
[**] Available from http://www.llnl.gov/CASC/linear_solvers/pubs.html.

DOI: 10.1002/fld

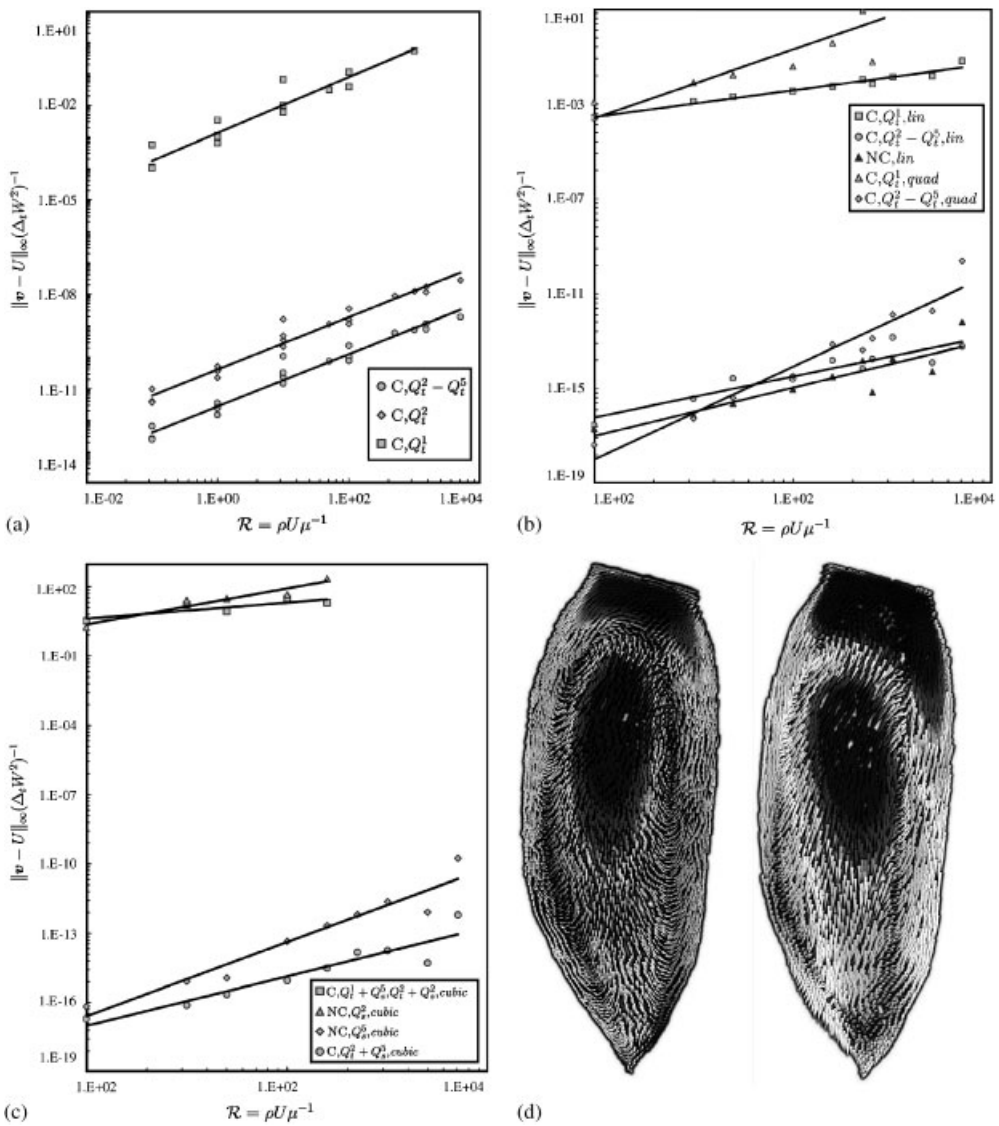

Figure 1. (a) Error for constant flow through a rectangular box, $\mathscr{T}_\Lambda$, at various $\mathscr{R}$ using $\mathbb{P}^2-\mathbb{P}^1$ Taylor–Hood elements for the state variables. Space was discretized using linears. Spatial quadrature is held fixed, with varying temporal quadrature (where Q_s^n, $n>5$). (b) Error for constant flow through a rectangular box, $\mathscr{H}_\Lambda$, at various $\mathscr{R}$ using $\mathbb{P}^2-\mathbb{P}^1$ Taylor–Hood elements for the state variables. Space was discretized using trilinears (lin) and triquadratics (quad). Spatial quadrature is held fixed, with varying temporal quadrature (where Q_s^n, $n>5$). (c) Error for constant flow through a rectangular box, $\mathscr{H}_\Lambda$, at various $\mathscr{R}$ using $\mathbb{P}^3-\mathbb{P}^2$ Taylor–Hood elements for the state variables. Space was discretized using tricubics (cubic). Spatial quadrature was given as an n-point Gaussian quadrature rule (Q_s^n), with varying temporal quadrature. (d) Cross section of 3D simulated ventricular flow at end diastole. Left: (c) Simulation showing two vortices, velocity magnitude (0 cm/s ~ white to 10 cm/s ~ black). Right: Vector cones showing difference in velocity with proper and improper integration, magnitude (0% velocity ~ white to 10% velocity ~ black).

DOI: 10.1002/fld

stress (outlet) boundary conditions were applied. With an initial velocity $\widehat{\mathbf{v}}(\Omega_0) = U(1,0,0)^{\mathrm{T}}$, these boundary conditions preserve constant flow. For comparison, the simulations were only run to the first time step (Δ_t).

The flow was discretized using tetrahedral ($\mathscr{T}_\Lambda$) and hexahedral elements ($\mathscr{H}_\Lambda$). The spatial discretization was taken as linear for $\mathscr{T}_\Lambda$, and linear/triquadratic/tricubic for $\mathscr{H}_\Lambda$. The velocity and pressure spaces (general Taylor–Hood [11]) were $\mathbb{P}^2-\mathbb{P}^1$ or $\mathbb{P}^3-\mathbb{P}^2$. Results for the (c) and (nc) forms were calculated under varying n-point spatial quadratures (Q_s^n), timescales (Δ_t), domain velocities ($W = \|\widehat{\mathbf{w}}\|_\infty$) and Reynolds numbers. Further, results for the (c) form were calculated for different temporal quadrature (Q_t^n, Q_t^2, or the hybrid $Q_t^2 + Q_t^5$ scheme of Section 2.2). Figure 1(a) and (b) plots the relationship of Reynolds number ($\mathscr{R}$) and the scaled error. Dimensionalization[††] of Equation (1) provided the relevant scaling as seen numerically.

All (c) forms but those with Q_t^2 or higher temporal quadrature lost stability for $\mathscr{R}W^2\Delta_t > 10^2$, regardless of element/basis selection. Schemes with Q_t^2 or higher temporal quadrature demonstrated improved accuracy and stability for $\mathscr{R}W^2\Delta_t \gg 10^5$. Further, using a higher quadrature form (Q_t^5) for the viscous terms resulted in a two-fold increase in accuracy. Additionally, both (c) and (nc) forms can demonstrate instability when the spatial quadrature rule is insufficient to satisfy the discretized SCL (RHS of Equations (4) and (6)) as seen in Figure 1(b).

Inclusion of $\mathrm{div}(\widehat{\mathbf{v}})$ terms to momentum showed no improvement in results. This is likely an artifact of the basis being able to capture the solenoidicity of the field due to its simplicity (i.e. constant flow) and is not expected for more complex flows.

Finally, we considered the (c) Q_t^1 and (c) $Q_t^2 + Q_t^5$ forms for ventricular flows. Figure 1(d), showing snapshots at the end of ventricular filling (end diastole), demonstrates the deleterious effects in solution accuracy due to improper conservation and spatio-temporal treatment.

4. CONCLUSION AND FUTURE WORK

As demonstrated, the difference in results between non-conservative and conservative schemes as well as their spatial and temporal treatments can have a negative impact on solution accuracy (Figure 1(a)) and stability. These results become more pronounced (Figure 1(d)) and difficult to discern as erroneous for complex flow problems. The methodology described in Section 2.2 is shown to vastly improve the solution accuracy (upwards of 12 orders of magnitude) and stability by considering the implicit conservative and non-conservative weak forms. This scheme provides a more rigorous and stable platform for considering these complex boundary-driven flows and their extension into coupled fluid–solid problems.

Characterizing ventricular fluid flow is increasingly important for clinical applications. Further, applications in tissue mechanics and fluid–solid coupling, which delves into the complex questions of feedback and control, is an important step in understanding heart physiology. Using the information developed here, we will integrate this ALE form of NSE with the tissue-based continuum-based model of Nash and Hunter [13].

[††]Dimensionalized according to the following scalings $(x, t, \mathbf{v}, \mathbf{w}, p) = (W\Delta_t, U, U, W, \rho U^2 \Delta_t^{-1})$.

DOI: 10.1002/fld

REFERENCES

1. McQueen DM, Peskin CS. A 3D computational method for blood flow in the heart. II. Contractile fibers. *Journal of Computational Physics* 1989; **82**:289–297.
2. Lemmon JD, Yoganathan AP. Computational modeling of left heart diastolic function: examination of ventricular dysfunction. *Journal of Elasticity* 2000; **122**:297–303.
3. Baccani B *et al*. Fluid dynamics of the left ventricular filling in dilated cardiomyopathy. *Journal of Biomechanics* 2002; **35**:665–671.
4. Cheng Y, Oertel H, Schenkel T. Fluid–structure coupled CFD simulation of the left ventricular flow during filling phase. *Annals of Biomedical Engineering* 2005; **8**:567–576.
5. Saber NR *et al*. Computational flow modeling of the left ventricle based on *in vivo* MRI data: initial experience. *Annals of Biomedical Engineering* 2001; **29**:275–283.
6. Watanabe H *et al*. Computer simulation of blood flow, left ventricular wall motion and their interrelationship by fluid–structure interaction finite element method. *JSME International Journal* 2002; **45**:1003–1012.
7. Malvern LE. *Introduction to the Mechanics of Continuous Medium*. Prentice-Hall: Englewood Cliffs, NJ, 1969.
8. Demirdžić I, Perić M. Space conservation law in finite volume calculations of fluid flow. *International Journal for Numerical Methods in Fluids* 1988; **8**:1037–1050.
9. Formaggia L, Nobile F. Stability analysis of second-order time accurate schemes for ALE–FEM. *Computer Methods in Applied Mechanics and Engineering* 2004; **193**:4097–4116.
10. Nobile F. Numerical approximation of fluid–structure interaction problems with application to haemodynamics. *Ph.D. Thesis*, École Polytechnique Fédérale de Lausanne, 2001; No. 2458.
11. Brezzi F, Falk RS. Stability of higher-order Hood–Taylor methods. *SIAM Journal on Numerical Analysis* 1991; **28**:581–590.
12. Dennis J, Schnabel R. *Numerical Methods for Unconstrained Optimization and Nonlinear Equations*. SIAM, Prentice-Hall: Philadelphia, PA, Englewood Cliffs, NJ, 1996.
13. Nash M. Hunter P. Computational mechanics of the heart. *Journal of Elasticity* 2000; **61**:113–141.
14. Liu Y, Vinokur M. Exact integration of polynomials and symmetric quadrature formulas over arbitrary polyhedral grids. *Journal of Computational Physics* 1998; **140**:122–147.

DOI: 10.1002/fld